Self-assembled nanoparticles based on cyclodextrin-modified pullulan

Synthesis, and structural characterization using SAXS

Stensgaard Diget, Jakob; Lund, Reidar; Nyström, Bo; Wintgens, Véronique; Amiel, Catherine; Wimmer, Reinhard; Terndrup Nielsen, Thorbjørn

Published in:
Carbohydrate Polymers

DOI (link to publication from Publisher):
10.1016/j.carbpol.2019.01.106

Publication date:
2019

Document Version
Accepted author manuscript, peer reviewed version

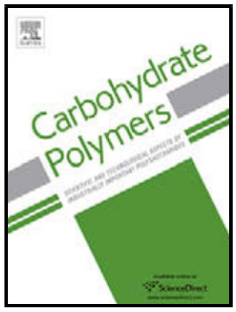

Title: Self-assembled nanoparticles based on cyclodextrin-modified pullulan: Synthesis, and structural characterization using SAXS

Authors: Jakob Stensgaard Diget, Reidar Lund, Bo Nyström, Véronique Wintgens, Catherine Amiel, Reinhard Wimmer, Thorbjørn Terndrup Nielsen

PII: S0144-8617(19)30119-5
DOI: https://doi.org/10.1016/j.carbpol.2019.01.106
Reference: CARP 14564

To appear in:

Received date: 27 November 2018
Revised date: 29 January 2019
Accepted date: 29 January 2019

Please cite this article as: Stensgaard Diget J, Lund R, Nyström B, Wintgens V, Amiel C, Wimmer R, Terndrup Nielsen T, Self-assembled nanoparticles based on cyclodextrin-modified pullulan: Synthesis, and structural characterization using SAXS, *Carbohydrate Polymers* (2019), https://doi.org/10.1016/j.carbpol.2019.01.106

Self-assembled nanoparticles based on cyclodextrin-modified pullulan: Synthesis, and structural characterization using SAXS

Jakob Stensgaard Diget[a], Reidar Lund[a], Bo Nyström[a], Véronique Wintgens[b], Catherine Amiel[b], Reinhard Wimmer[c] and Thorbjørn Terndrup Nielsen[c]*

[a]Department of Chemistry, University of Oslo, P.O.Box 1033, Blindern, N-0315 Oslo, Norway. [b]Université Paris Est, ICMPE (UMR7182), CNRS, UPEC, F 94320 Thiais, France. [c]Department of Chemistry and Bioscience, Aalborg University, Fredrik Bajers Vej 7H, 9220 Aalborg Ø, Denmark

* To whom correspondence should be addressed; ttn@bio.aau.dk

Graphical abstract

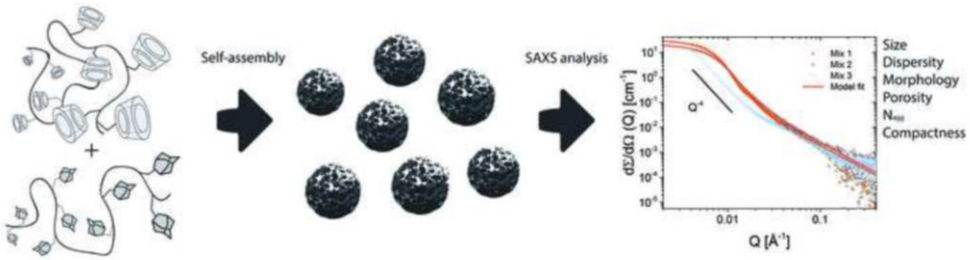

Highlights

- Pullulan was modified with β-cyclodextrin via "click" chemistry
- Nanoparticles were created via self-assembly with an adamantane-modified dextran
- The sub-100 nm particles were characterized using small-angle X-ray scattering (SAXS)
- Polymer molecular structure and host-guest ratio strongly affected particle properties

Abstract

Synthesis of novel host-guest functionalized polymers is presented along with structural characterization using small-angle X-ray scattering (SAXS) of the resulting nanoparticles. Mono-6-deoxy-mono-6-azidoβCD (N_3βCD) was grafted onto alkyne-functionalized pullulan via the "click" reaction copper(I)-catalyzed azide alkyne cycloaddition (CuAAC) and an adamantane-modified dextran was prepared via the same strategy. Characterization of the polymers was carried out using nuclear magnetic resonance (NMR) spectroscopy, gel filtration chromatography (GFC), isothermal titration calorimetry (ITC) and SAXS. Nanoparticles were created via host-guest interactions between the well-defined βCD-pullulans and adamantane-modified dextran. Characterization was carried out using dynamic light scattering (DLS) and SAXS, which revealed spherical particles in the sub-100 nm range. The studies shed light on the

importance of molecular structure and host-guest ratio on crucial properties such as particle size, size distribution, porosity and stability towards aggregation.

Keywords: Pullulan; β-cyclodextrin (βCD); "click" chemistry; self-assembly; host-guest chemistry; small-angle X-ray scattering (SAXS).

1. Introduction

Cyclodextrin polymers (CD-polymers) have attained numerous applications in the last decades in such various fields as water remediation (Alsbaiee et al., 2016; Morin-Crini et al., 2018; Wang, Zhang, Hu, Zhao, & Zhu, 2017; Xiao et al., 2017), hydrogels for drug delivery (K Osman, M Soliman, & Abd El Rasoul, 2015; Machín, Isasi, & Vélaz, 2012; Malik, Ahmad, & Minhas, 2017), nanosponges (Trotta, Zanetti, & Cavalli, 2012) and stimuli responsive and self-healing materials (Jia & Zhu, 2014; Kakuta, Takashima, & Harada, 2013; Takashima et al., 2012). In recent years the use of CD conjugated biopolymers for biomedical applications has gained increasing attention. These e.g. include CD conjugated to alginate (Gomez, Chambat, Heyraud, Villar, & Auzély-Velty, 2006), hyaluronic acid (Charlot, Heyraud, Guenot, Rinaudo, & Auzély-Velty, 2006), chitosan (Lu, Shao, Jiao, & Zhou, 2014) and dextran (Nielsen, Wintgens, Amiel, Wimmer, & Larsen, 2010). Pullulan is linear biocompatible non-toxic, non-immunogenic and non-mutagenic natural occurring polysaccharide similar to dextran, also consisting of D-glucose units (Singh, Kaur, Rana, & Kennedy, 2017). The difference from dextran lies in the way the glucose units are connected. In dextran they are connected through α-1,6 glycosidic bonds with some branching through α-1,3 glycosidic bonds, whereas pullulan consists of

maltotriose units connected through α-1,4 glycosidic bonds (Bender, Lehmann, & Wallenfels, 1959; Shingel, 2004). Even though the polymers have the same repeating units and chemical formula, the different connectivity results in different properties. A comparative study was made on the degradability of pullulan vs. dextran where it was found that pullulan was more easily degraded (Bruneel & Schacht, 1995). From nuclear magnetic resonance (NMR) spectroscopy it has also been shown that the flexibility is higher for dextran since the connections through the α-1,6 glycosidic bonds are more flexible than those of the α-1,4 glycosidic bonds in pullulan (Brant, Liu, & Zhu, 1995; Dais, Vlachou, & Taravel, 2001; Kadkhodaei, Wu, & Brant, 1991). The connections in pullulan moreover lead to a slight helical twist, mimicking the behavior of amylose (Buliga & Brant, 1987; Burton & Brant, 1983). Pullulan and derivatized pullulan have been used as a human blood plasma substitute since 1944 and in treatment of hepatitis, respectively (Whistler, 2012). More recently, pullulan based nanoplatforms for delivery of the anticancer agent mitoxantrone were developed by coupling βCD and polyethyleneimine to a pullulan (Mitha & Rekha, 2014). Also, cross-linked pullulan-CD nanospheres for chromatography (Fundueanu et al., 2003) have been prepared but the reports of pullulan-CD conjugates remain scarce.

Previously we have applied copper(I)-catalyzed alkyne-azide cycloaddition (CuAAC) (Rostovtsev, Green, Fokin, & Sharpless, 2002; Tornøe, Christensen, & Meldal, 2002), to covalently attach βCD to dextran (Nielsen et al., 2010). Also on dextran, the same procedure was employed to covalently attach adamantane (Layre, Volet, Wintgens, & Amiel, 2009). In later work, the two polymers were mixed to form well-defined nanoassemblies through βCD-adamantyl host-guest interactions (Antoniuk et al., 2017; Wintgens, Nielsen, Larsen, & Amiel, 2011). Because of the increasing interest in such systems for drug-delivery purposes, it is highly

desired to develop suitable polymers that allow control of the resulting nanoassemblies, and to gain a better understanding of how these assemblies can be tailored. In the current study, CuAAC was applied for the synthesis of novel βCD and adamantane modified pullulan and dextran, respectively. Pullulan was chosen because of its attractive properties in e.g., drug delivery, where it has shown hemocompatibility and affinity for liver cells (Kaneo, Tanaka, Nakano, & Yamaguchi, 2001; Rekha & Sharma, 2011; Tanaka, Fujishima, Hanano, & Kaneo, 2004), whereas dextran has many of the same properties but lack target delivery. The reason to include dextran was to introduce more flexibility in the subsequent nanoparticle formation; thus increasing the change of the host-guest moieties to meet and thus form stable nanoparticles. Molecular structure, molar mass, dispersity ($Đ_M = M_w/M_n$) and binding properties of the polymers were determined using NMR spectroscopy, gel filtration chromatography (GFC) and isothermal titration calorimetry (ITC). Nanoparticles were obtained by simply mixing the well-defined host-guest polymers in aqueous solution. The nanoparticles were thoroughly characterized using dynamic light scattering (DLS) and SAXS.

2. Materials and methods

2.1 Materials

Acetone (VWR, Haasrode, Belgium), ammonia solution 25% (Merck, Darmstadt, Germany), dimethyl sulfoxide (DMSO, Fischer Scientific, Loughborough, United Kingdom), (+)-sodium L-ascorbate 99% (NaAsc, Fluka, Steinheim, Germany), copper(II) sulfate 99%

(Fluka, Steinheim, Germany), dextran T70 (D70, weight average molar mass (M_w) 65 kg mol^{-1}, $Đ_M$ 1.314, Pharmacosmos A/S, Holbaek, Denmark), pullulan (PL, M_w 112 kg mol^{-1}, $Đ_M$ 1.575, Hayashibara Company Ltd, Okayama, Japan), Ambersep GT74 (Supelco, Bellefonte, USA), ethyl acetate, 2-propanol puriss, diethyl ether >99.9%, dichloromethane ≥ 99.8%, sodium hydroxide ≥ 98%, *N,N*-dimethylformamide puriss >99.8%, glycidyl propargyl ether (GP) technical ≥ 90%, triethylamine >99% (all from Aldrich, Steinheim, Germany).

Mono-6-deoxy-mono-6-azido-βCD (N_3βCD) (Nielsen et al., 2010), alkyne-functionalized dextran (D70Hx, where Hx denotes the hexynoyl group) (Nielsen et al., 2010), tris((1-benzyl- 1,2,3-triazol-4-yl)methyl)amine (TBTA) (Chan, Hilgraf, Sharpless, & Fokin, 2004) and azidomethyl adamantane (N_3Ada) (Foot, Lui, & Kluger, 2009) were prepared as described in literature.

2.2 Characterization

NMR experiments were performed on a BRUKER AVIII-600 MHz NMR spectrometer equipped with a CPP-TCI cryogenically cooled probe. Spectra were recorded and processed with TopSpin 3.5pl6. ^{1}H-NMR, [^{1}H,^{1}H] double quantum filtered (DQF) correlation spectroscopy (COSY) and [^{1}H,^{13}C] heteronuclear single quantum coherence (HSQC) NMR spectra were recorded. Spectra were calibrated according to the residual solvent signal. For those obtained in D_2O, HDO was calibrated according to a temperature dependent formula (Gottlieb, Kotlyar, & Nudelman, 1997). Chemical shifts in the remainder of the text are reported at 310 K. ^{1}H and ^{13}C NMR signals of the glucose units of pullulan, dextran and βCD, are reported as H1-H6 and C1-C6, respectively, where 1-6 refer to the position in the glucose units (1 and 6 indicating the anomeric position and the CH_2, respectively). The content of functional groups in the polymers

were calculated using the integrals of the characteristic ^{1}H NMR signals of H1 and the alkyne- or triazol groups, before or after CuAAC, respectively, and is described in detail later. GFC, coupled to a multi-angle laser light scattering detector for absolute molar mass determination, was carried out in deionized water with 0.1 mol L^{-1} lithium nitrate and 0.05% wt. sodium azide (TSK-gel SW 4000-3000 column and detection by a Wyatt Dawn 8+ light scattering detector and a Wyatt Optilab Rex refractive index detector). DLS was carried out on a Zetasizer Nano-ZS (Malvern Instrument) equipped with a helium-neon laser (λ = 633 nm, scattering angle 173°). Samples were measured ten times for ten seconds at 25 °C, and the measurements were made in duplicate. The reported mean value (or Z-average size) and the size distribution were obtained using cumulant analysis (fit of the logarithm of the correlation function by a 3rd order polynomial). ITC measurements were carried out at 25 °C in 0.1 mol L^{-1} sodium chloride using a MicroCal VP-ITC microcalorimeter, as previously reported for titrations of βCD polymers (Nielsen et al., 2010). The experimental data were fitted with a theoretical titration curve corresponding to a 1:1 complex formation, using the software developed by MicroCal. The enthalpy change, ΔH, association constant, K, and the overall stoichiometry, n, were used as adjustable parameters. SAXS experiments were performed using the automated BM29 bioSAXS beamline at the European Synchrotron Radiation Facility (ESRF), Grenoble, France. Technical details can be found in the work of Pernot et al. (Pernot et al., 2013). The experiments were carried out using an energy of 12.5 keV and detector distance 2.87 m covering a Q-range ($Q = 4\pi \sin(\theta/2)/\lambda$, where λ = 1.54 Å is the wavelength, θ is the scattering angle) of about 0.0047 $Å^{-1} < Q < 0.5$ $Å^{-1}$. The data were calibrated to absolute intensity scale using water as a primary standard. The solution density in water, required to estimate the scattering length density/contrast

in the SAXS modeling, was measured at 0.5 wt. % for the adamantane-modified dextran, and 1 wt. % for the βCD-modified pullulans using an AntonPaar DMA 5000 densitometer.

2.3 Theoretical modeling of SAXS data

The scattering from the (unmixed) polymer solutions was described using the Beaucage form factor (Beaucage, 1996) as follows:

$$I(Q)_{polymer} = \varphi \cdot M_w/d_p \cdot (\rho_P - \rho_0)^2 \left(\exp\left(-\frac{Q^2 \cdot R_g^2}{3}\right) + \frac{d_f}{(Q \cdot R_g)^{d_f}} \Gamma\left(\frac{d_f}{2}\right) \cdot \left(\frac{[erf\left(\frac{Q \cdot Rg}{\sqrt{6}}\right)]^3}{Q} \right)^{d_f} \right) \quad (1)$$

Where $\varphi = c/d_0$ is the volume fraction of polymer, with d_0 being the density of the solution and c the concentration in g mL^{-1}, M_w the polymer molecular weight, $Q = 4\pi \sin\left(\frac{\theta}{2}\right)/\lambda$ is the scattering vector, λ the wavelength of the X-rays, θ is the scattering angle, R_g is the radius of gyration, d_f is the fractal dimension (d_f = 2 and 1.7 for theta solvent and good solvent, respectively) and d_p is the density of the polymer. $\Gamma(x)$ is the gamma function and $erf(x)$ is the error function. The scattering length density (ρ_0 and ρ_p for the solvent and polymer, respectively) was calculated according to:

$$\rho = \frac{N_A \sum_i Z_i}{\overline{M/d}} r_0 \quad (2)$$

where Z_i is the number of electrons, M is the molecular weight of the average polymer repeat unit or solvent molecule, while d is the corresponding density (d_0 and d_p for the density of the solution and polymer, respectively), N_A Avogadro's number and r_0 is the Bohr radius.

The scattering from a nanoparticle (abbreviated NP in the equations) was modeled as a spherical object of mean size $\langle R_p \rangle$ with "fuzzy" outer surface characterized by a roughness parameter, σ_R.

The latter was included by performing a convolution over the interface of the spheres, which together with assuming a Gaussian distribution of nanoparticle size, gives the following expression for the total scattered intensity:

$$\langle I(Q)\rangle_{NP} = \frac{\varphi}{\langle V\rangle}(\rho_P - \rho_0)^2 \int_0^\infty V(r)^2 f(r) P(Q,r)_{NP} dr \qquad (3)$$

The form factor for individual fuzzy spheres of radius, r, can be written as:

$$P(Q,r)_{NP} = \left[\frac{3\cdot(\sin(Q\cdot r) - Q\cdot r\cdot\cos(Q\cdot r)}{(Q\cdot r)^3}\right]^2 \cdot \exp^{(-Q^2\cdot\sigma_R{}^2)} \qquad (4)$$

The corresponding size distribution, *f(r)* is given by:

$$f(r) = \frac{1}{\sqrt{2\pi\cdot\sigma_{PD}}} exp(-\frac{(r-\langle R_p\rangle)^2}{2\sigma_{PD}{}^2} \qquad (5)$$

where σ_{PD} is the Gaussian width of the particle distribution and $\langle R_p\rangle$ is the mean nanoparticle size. The volume of a nanoparticle is given by:

$$\langle V\rangle = \int_0^\infty V(r) f(r) dr \qquad (6)$$

where $V(r)$ is the volume occupied by polymers within each nanoparticle of radius r: $V(r) = 4\pi r^3/3\cdot(1\text{-}\Phi_0)$. For simplicity we assume that the amount of solvent within the particle is independent of size and given by:

$$\Phi_0 = 1 - \frac{M_{NP}}{\langle \boldsymbol{V}\rangle d_p} \qquad (7)$$

where M_{NP} is the weight-average molar mass of the nanoparticles and d_p is the mean density of the polymers. The density profile of the nanoparticle can then be calculated according to:

$$n(r) = (1 - \Phi_0) \int_0^\infty \theta\big((r - r' - R_p\big) \frac{1}{\sqrt{2\pi\sigma_R^2}} \exp\big(-(r' - R_p)^2/2\sigma_R^2\big) dr \quad (8)$$

Where r' is a dummy variable and the "step function" was chosen to be: $\theta(x) = 0.5 - \tanh(kx)$, where k =1000.

In account for the swelling of the nanoparticles, we must include the internal polymer-like scattering contribution by adding a "blob scattering" term to the total scattering:

$$I\,(Q) = \langle I(Q)\rangle_{NP} + I(Q)_{blob} \quad (9)$$

The blob scattering can be described by a polymer-like contribution at high Q and is parameterized by a Lorentzian term:

$$I(Q)_{blob} = \frac{I_0}{(1+Q^2\xi^2)} \quad (10)$$

where I_0 is a prefactor in units of cm^{-1} and ξ is a "mesh" size of the internal polymer network.

2.4 Synthesis

PLGP and PLGPβCD were synthesized according to a previously described method for βCD-modified dextran (Nielsen et al., 2010). D70HxAda was synthesized according to the same procedure as PLGPβCD, with the exception of using DMSO as solvent to facilitate dissolution of azido-adamantane. One D70HxAda and four PLGPβCDs were synthesized. For the PLGPs, 10, 20, 30 and 40 mol% glycidyl propargyl ether of the total moles of glucose units in pullulan was

added. The PLGPβCDs were synthesized using an [alkyne : azide : $CuSO_4$: TBTA : NaAsc] mole ratio of [1 : 2 : 0.05 : 0.055 : 0.15]. Cf. the ESI for an overview of added amounts for all pullulans (table S1 and S2).

2.4.1 PLGP

Pullulan (3 g, 0.027 mmol) was dissolved in 15 mL 0.5 M aqueous sodium hydroxide. Glycidyl propargyl ether (208 mg, 1.852 mmol) was added, and the reaction was left stirred overnight at 35 °C. The polymer was precipitated in 2-propanol, filtered through a glass-sintered funnel, dissolved in water and dialyzed (6-8 kDa M_w cut-off) against demineralized water for 72 hours. The dialyzed polymer solution was filtered through a syringe filter (0.45 μm cutoff) and freeze-dried (2.8 g, 89% yield). PLGP: ^{1}H NMR (D_2O, 600 MHz): δ_H (ppm) PL: 5.74-4.89 (br, 1H, H1); 4.04-3.42 (br, 4H, H2-H5); 3.96-3.73 (br, 2H, H6): GP: 4.26 (s, 2H, O-$\underline{CH_2}$-alkyne); 4.09 (br, 1H, -CH_2-$\underline{CH}$(OH)-CH_2-); 3.78 and 3.73-3.59 (br, 4H, -$\underline{CH_2}$-CH(OH)-$\underline{CH_2}$-); 2.94 (s, 1H, alkyne): ^{13}C NMR (D_2O, 600 MHz): δ_C (ppm) PL: 104-99 (1C, C1); 83.4-71.6 (4C, C2-C5); 69.5 and 63.6 (1C, C6): GP: 79.3 (1C, alkyne); 75.4 and 73.8 (2C, -$\underline{CH_2}$-CH(OH)-$\underline{CH_2}$-); 72 (1C, -CH_2-$\underline{CH}$(OH)-CH_2-); 61.3 (1C, O-$\underline{CH_2}$-alkyne).

2.4.2 PLGPβCD

Alkyne-functionalized pullulan (PLGP, 0.25 g, 96 μmol alkyne), TBTA (147 μL of a 20 mg mL^{-1} solution in DMSO, 5.28 μmol) and mono-functionalized N_3βCD (0.223 g, 192 μmol) were dissolved in 25 mL degassed DMSO:water (1:1 v/v) under inert atmosphere. NaAsc (143 μL of a 20 mg mL^{-1} aqueous solution, 14.4 μmol) was added, and the solution was degassed using ultrasonication and subsequent purging with nitrogen for 10 min while heating the solution to 50

°C. Copper(II) sulfate (77 µL of a 10 mg mL^{-1} aqueous solution, 4.8 µmol) was added and the solution was stirred for 24 hours under inert atmosphere. The resulting polymer was precipitated in 500 mL 2-propanol and filtered through a glass-sintered funnel. The filtrate was washed twice with 150 mL 2-propanol and left drying over night. To remove residual copper, the polymer was re-dissolved in water and swirled over Ambersep GT74 resin for 12 hours. The polymer solution was then dialyzed against demineralized water for 72 hours, passed through a syringe filter (0.45 µm cutoff) and freeze-dried (white fluffy solid, 0.35 g, 97% yield). PLGPβCD: ^{1}H NMR (D_2O, 600 MHz): δ_H (ppm) PL: 5.36 and 4.94 (br, 1H, H1); 4.1-3.34 (br, 4H, H2-H5); 4.04-3.72 (br, 2H, H6): GP: 8.09 (s, 1H, CH group in triazol); 4.71 (br, 2H, PL-O-$\underline{CH_2}$-triazol); 4.06 (br, 1H, -CH_2-$\underline{CH}$(OH)-CH_2-); 3.74 and 3.72-3.61 (br, 4H, -$\underline{CH_2}$-CH(OH)-$\underline{CH_2}$-): βCD: 5.24-4.97 (br, 1H, H1); 5.02/4.64, 4.04-3.73, 3.2/2.88 (br, 2H, H6); 4.24-3.44 (br, 4H, H2-H5): ^{13}C NMR (D_2O, 600 MHz): δ_C (ppm) PL: 103.5-100.5 (1C, C1); 86.2-71.7 (4C, C2-C5); 69.5 and 63.6 (1C, C6): GP: 129.7 (1C, CH group in triazol); 75.5 and 74.3 (2C, $\underline{CH_2}$-CH(OH)-$\underline{CH_2}$-); 72 (1C, -CH_2-$\underline{CH}$(OH)-CH_2-); 66.6 (O-$\underline{CH_2}$-triazol): βCD: 105.2-104.2 (1C, C1); 86.2-71.7 (4C, C2-C5); 54.2, 63.5 and 62.3 (1C, C6).

2.4.3 D70HxAda

Alkyne-functionalized dextran (D70Hx, 0.3 g, 9.2% mole modified glucose units, 162 µmol alkyne), N_3Ada (130 mg, 323 µmol), and TBTA (621 µL of an 8 mg mL^{-1} solution in DMSO, 8.89 µmol) were dissolved in 25 mL of degassed DMSO under inert atmosphere. NaAsc (240 µL of a 20 mg mL^{-1} solution in DMSO, 24.3 µmol) was added and the solution was degassed by ultrasonication and subsequent purging with nitrogen for 10 min while heating to 50 °C.

Copper(II) sulfate (129 µL of a 10 mg mL^{-1} in DMSO, 8.1 µmol) was added and the solution was stirred for 24 hours under inert atmosphere. The resulting polymer was precipitated in 400 mL 2-propanol and filtered through a glass-sintered funnel. The filtrate was washed with 100 mL 2-propanol, then 50 ml acetone, and left to dry over night. The dried polymer was dissolved in water and swirled over Ambersep GT74 resin for 12 hours to remove remaining copper. The polymer solution was then dialyzed against demineralized water for 72 hours, filtered through a syringe filter (0.45 µm cutoff) and freeze-dried (white solid, 0.285 g, 78% yield). D70HxAda: ^{1}H NMR (DMSO-d_6, 600 MHz): δ_H (ppm) D70: 4.82 (d, 1H, OH attached to C4); 4.73 (d, 1H, OH attached to C3); 4.69 (d, 1H, H1); 4.36 (d, 1H, OH attached to C2); 3.76 and 3.52 (br, 2H, H6 splitting); 3.65 (br, 1H, H5); 3.44 (t, 1H, H3); 3.23 (br, 1H, H2); 3.19 (br, 1H, H4): Hx: 7.72 (s, 1H, CH group in triazol); 2.67 (t, 2H, triazol-$\underline{CH_2}$-); 2.37 (t, 2H, -$\underline{CH_2}$-C(O)-O-); 1.88 (p, 2H, -CH_2-$\underline{CH_2}$-CH_2-): Ada: 3.99 (s, 2H, Ada-$\underline{CH_2}$-triazol); 1.93 (br, 3H, CH); 1.68-1.5 (br, 6H, CH_2); 1.44 (br, 6H, CH_2). ^{13}C NMR (DMSO-d_6, 600 MHz): δ_C (ppm) D70: 98.8 (1C, C1); 73.8 (1C, C3); 72.3 (1C, C2); 70.9 (1C, C5); 70.6 (1C, C4); 66.6 (1C, C6): Hx: 124.5 (1C, CH group in triazol); 33.5 (1C, -$\underline{CH_2}$-C(O)-O-); 24.8 (1C, -CH_2-$\underline{CH_2}$-CH_2-); 24.6 (1C, triazol-$\underline{CH_2}$-): Ada: 61.3 (Ada-$\underline{CH_2}$-triazol); 40.2 (3C, CH_2); 36.6 (3C, CH_2); 28 (3C, CH).

3. Results and discussion

Pullulan and dextran were successfully functionalized with alkynes, followed by "clicking" the host (βCD) and guest (Ada) functionalities onto the polymers, cf. figure 1 for an illustration of the synthesis.

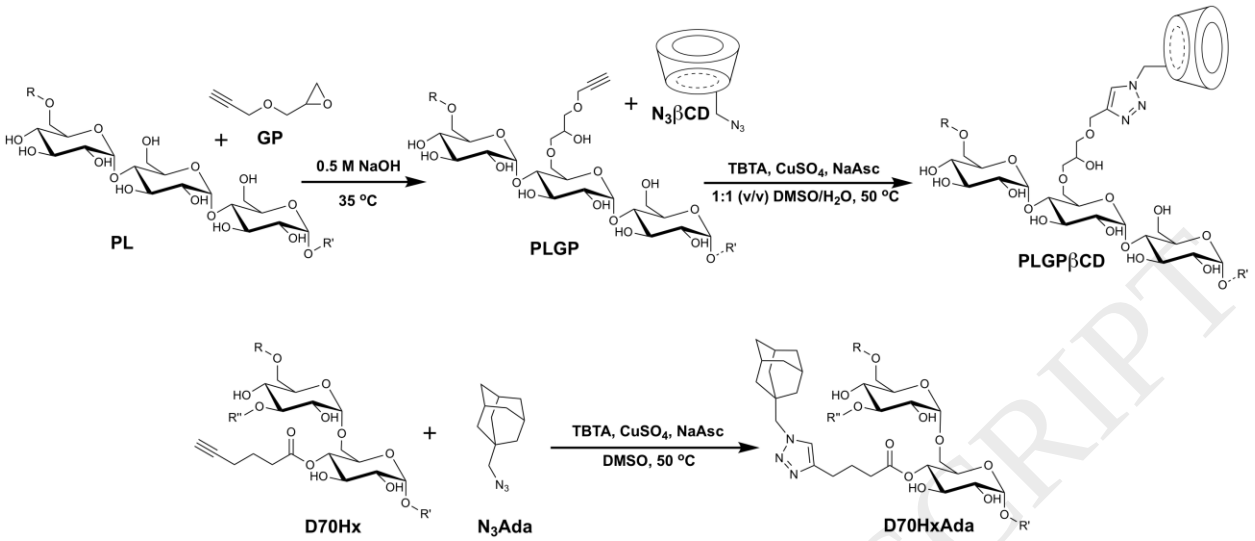

Fig. 1. Synthesis scheme of PLGPβCD (top) and D70HxAda (bottom). R-groups indicate continuation of the polymers, where R'' indicates the small amount of branching through α1,3 glycosidic bonds. Modification is shown on the primary OH of pullulan and on the OH attached to C4 of dextran for simplicity; however, modification of the glucose units is statistically distributed on all accessible OH groups, determined by reactivity and accessibility.

Pullulan was successfully modified with glycidyl propargyl ether via a simple one-step nucleophilic epoxide opening under basic conditions in water. On average, 63% of the added glycidyl propargyl ether was incorporated (aim 10-40%, obtained 6.5-23.6%), as a result of competing hydrolysis of the epoxide. This however, is significantly more than reported for the modification of dextran, where 41% was incorporated following the same procedure (Nielsen et al., 2010). The reason for this difference is that the more reactive primary hydroxyl groups are accessible for modification in pullulan, whereas this is not the case in dextran (glucose units connected through α1,6 glycosidic bonds). D70Hx was therefore synthesized using an acylation procedure, which has previously shown to be more effective than the glycidyl propargyl ether approach on dextran (Nielsen et al., 2010). However, as it involves several synthesis steps, it was

only used for the modification of dextran. Using that procedure, 74% of the added alkynes (hexynoyl chloride) were incorporated (aim 12.5%, obtained 9.2%).

The subsequent CuAACs between the alkyne-functionalized polymers and the azide moieties (N_3βCD and N_3Ada) resulted in high yields (93-97% and 78% for PLGPβCD and D70HxAda, respectively) and complete conversion of the alkynes, cf. figure 2 showing the ^{1}H NMR spectra of the purified PLGP4, D70Hx, PLGPβCD4 and D70HxAda. As seen from the spectra, the alkyne signals of PLGP4 and D70Hx are absent in PLGPβCD4 and D70HxAda and triazol signals (with same integral values) have emerged. The % modified glucose units of the polymeric backbones was found using the integrals of the anomeric protons, H1, and those of the alkynes or triazoles. These integrals could be directly used for PLGP, D70Hx and D70HxAda (therefore calibrated to 100 giving the % modification from the alkyne or triazol integrals), whereas for the PLGPβCDs the anomeric PL protons overlap with those of the βCD and one proton from the H6 CH_2 group of βCD carrying the triazol, and was therefore taken into account in the calculations. A complete NMR assignment is given in the synthesis section, and ^{1}H NMR spectra of all polymers, along with 2D NMR spectra used for elucidation, are found in the ESI.

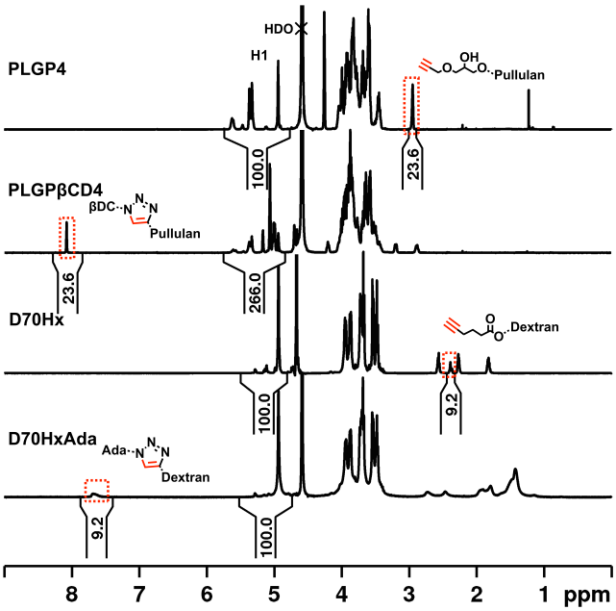

Fig. 2. ^{1}H NMR spectra of PLGP4, PLGPβCD4, D70Hx and D70HxAda obtained in D_2O. Integrals of the alkynes and triazoles directly indicate the mole % modified glucose units of the polymer backbone.

The M_w and $Đ_M$ of the final polymers (PLGPβCDs and D70HxAda) were determined using GFC, and the M_w also with SAXS for PLGPβCD4 and D70HxAda (SAXS results explained later). The GFC results and mole- and wt. % modification along with number of βCD or Ada per polymer chain (Units/chain), calculated based on ^{1}H NMR results, are found in table 1. Degree of modification was controlled by simply varying the feed ratio of alkyne to glucose units in pullulan.

Table 1. M_w [kg mol^{-1}] and $Đ_M$, obtained using GFC analysis, of polymers along with mole- and wt. % modification and number of βCD or Ada per polymer chain (Units/chain), calculated from ^{1}H NMR data.

	Mole % βCD or Ada[a]	Wt. % βCD or Ada[b]	Units/chain	M_w (GFC)	$Đ_M$ (GFC)
PLGPβCD1	6.5	29.9	44	119	1.57
PLGPβCD2	12.9	44.7	89	180	1.56
PLGPβCD3	19.7	54.0	136	247	1.52
PLGPβCD4	23.6	57.8	163	279	1.54

D70HxAda	9.2	8.6	37	N/A	N/A

[a]Mole % βCD or Ada was calculated using the ^{1}H NMR integrals of the protons attached to the anomeric carbon, i.e., the protons of position 1 in the glucose units (H1), and the signal of the triazol, and indicate the average % mole modified glucose units of the pullulan (M_w = 112 kg mol^{-1}, 691 repeating units) or dextran (M_w = 65 kg mol^{-1}, 401 repeating units). [b]Calculated as [Mole % βCD] x M_w(N_3βCD) / ([Mole % βCD] x (M_w(N_3βCD) + M_w(GP)) + (M_w(glucose) – M_w(H_2O))). Same approach was used for the calculation of the wt. % modification of D70HxAda.

To test the ability of the PLGPβCDs to form inclusion complexes, the interactions between the host polymers and a guest molecule, 2-(1-adamantyl)ethyl trimethyl ammonium bromide (AdaTMA), were measured using ITC. The association constants of 1.1-1.8 10^5 L mol^{-1}, thus obtained, are comparable to those reported for βCD-modified dextrans with βCD being grafted through the same type of spacer as used in the current study (GP) (Nielsen et al., 2010). The complex formation is strongly exothermic and enthalpy driven with high |ΔH| values, around 32.6-34.5 kJ mol^{-1}, which is expected for a complex formation between βCD cavities and an adamantane derivative (Rekharsky & Inoue, 1998). This high binding constant is similar to the one obtained for native βCD (1.9 10^5 L mol^{-1}), showing the great accessibility of the βCD cavities. The thermodynamic parameters for inclusion complex formation between AdaTMA and the PLGPβCDs can be found in the supplementary data (table S3) along with the enthalpograms of the titrations (figure S26 and S27).

With the verified host properties, we proceeded to create host-guest nanoparticles. Polymer solutions were mixed, 1:1 v/v (βCD and adamantyl concentration in solutions are 0.45 μM), under mild stirring and the size was monitored over 24 hours with DLS at room temperature. As is clear from the results, cf. table 2, mixing equimolar dilute solutions of the host:guest moieties of the βCD/adamantane-modified polymers leads to the formation of uniform nanoparticle size distributions (dispersities of 0.025-0.08). It is also seen that the higher the mole % modified glucose units of the βCD-polymer backbone, the smaller the size and more stable the

nanoparticles are. A similar trend has previously been described for βCD-modified dextran (Wintgens et al., 2011), and may possibly be explained by a more rigid and dense network formation with increasing modification densities of host and guest molecules.

Table 2. Diameter (no bracket, in nm) and dispersity/polydispersity index (in brackets), measured using DLS, as a function of time for nanoparticles of PLGPβCD1-4 mixed with D70HxAda (1:1 molar ratio of βCD:Ada). Table entries are named with the PLGPβCDs of the nanoparticles for simplicity.

	0 hours	1.5 hours	3 hours	7 hours	24 hours
PLGPβCD1[a]	88.3 (0.066)	92 (0.047)	97.8 (0.029)	101.8 (0.027)	111.9 (0.025)
PLGPβCD2[b]	66.3 (0.075)	68.5 (0.049)	70.4 (0.051)	70.7 (0.063)	75.7 (0.065)
PLGPβCD3[c]	64. 8(0.050)	67.9 (0.037)	69 (0.068)	70.8 (0.039)	73.8 (0.030)
PLGPβCD4[d]	62.9 (0.080)	66.3 (0.062)	67.2 (0.045)	67.9 (0.044)	70.8 (0.031)

[a,b,c,d]Equimolar βCD:Ada mixes, obtained by mixing 1:1 (v/v) of either 1.69, 1.14, 0.943 and 0.881 mg mL^{-1} PLGPβCD1, 2, 3 and 4, respectively, with 0.922 mg mL^{-1} D70HxAda. All concentrations correspond to 0.45 μM βCD or Ada.

In order to elucidate the detailed nanostructure, including the internal density distribution, the nanoparticles of PLGPβCD4 and D70HxAda were investigated in detail using SAXS as the overall sizes of these were smallest and therefore most suitable for the structural resolution of this technique. The formation of nanoparticles is illustrated in figure 3, where the scattered intensity of the molecularly dissolved (unmixed) polymers, PLGPβCD4 and D70HxAda (0.881 and 0.922 mg mL^{-1}, respectively, corresponding to a βCD and adamantyl concentration of 0.45 μM), is compared with a mixed sample with equimolar host:guest ratio (denoted mix 1, prepared by mixing 1:1 (v/v)).

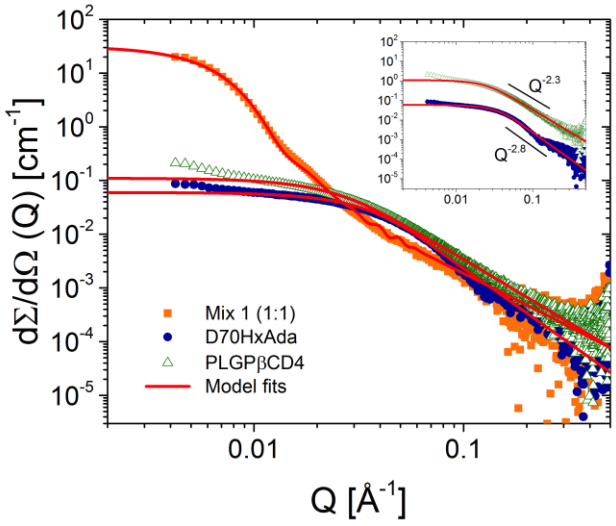

Fig. 3. SAXS intensity as a function of the modulus of the scattering vector, Q, of the PLGPβCD4 and D70HxAda reservoirs and a 1:1 host:guest ratio mixed sample (mix 1). Insert shows the same data for PLGPβCD4 and D70HxAda where the former has been shifted by a factor 10 for better visibility. The solid lines display model fits.

As seen, the scattered intensity increases by a factor of about 100 at low Q upon mixing the polymers. Moreover, the data display a rather well-defined shoulder and hints of oscillations at intermediate Q-values, indicating the formation of well-defined nanoparticles. In contrast, for the individual reservoirs, we observe polymer-like scattering with a smooth decay at high Q. A comparison using a generalized polymer scattering model (equation 1 in section 2.3) shows that, while PLGPβCD4 is nicely described with this model, there are deviations at high Q for D70HxAda. This might be a sign of local structuring and intra- /inter-molecular hydrophobic interactions leading to more compact local domains. At low Q a rather clear Guinier-like regime is observed, but at lowest values an upturn is seen, indicating that the polymer solutions are not completely homogenous, which further indicates the formation of large clusters. Performing the SAXS analysis on an absolute intensity scale, we extract M_w = 242 kg mol^{-1}, R_g = 6.6 nm and d_f = 2.3 for PLGPβCD4 and M_w = 98 kg mol^{-1}, R_g = 4.4 nm and d_f = 2.8 for D70HxAda. Values of

PLGPβCD4 are as expected, where the d_f value of 2.3 indicates a branched polymer or network. This seems reasonable as the linear pullulan is randomly modified on 23.6 mole % of the glucose units with the relatively large βCD, rendering it a branched-type polymer. The M_w of 242 kg mol^{-1} obtained from the fit parameters also matches the one obtained from the GFC measurements (280 kg mol^{-1}) rather well.

The relatively large d_f of 2.8 and M_w of 98 kg mol^{-1} for D70HxAda reflects the clustering and was further substantiated by DLS analysis of D70HxAda, which revealed an increase in size over time. GPC was therefore not carried out. Instead a more precise M_w of 76.5 kg mol^{-1} was calculated based on the M_w of D70, obtained using GFC, and the degree of modification obtained from ^{1}H NMR and was therefore used for the calculation of N_{agg}, described later.

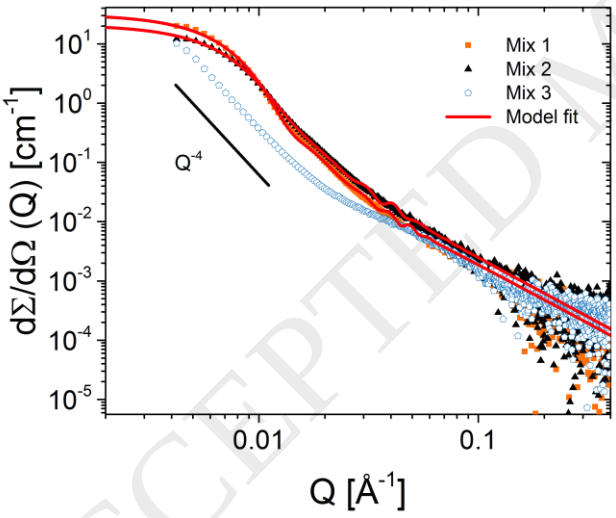

Fig. 4. SAXS intensity of PLGPβCD4 and D70HxAda mixed in different host:guest ratios: mix 1 (1:1), 2 (2.3:1) and 3 (1:2.3) (βCD:Ada molar ratio), respectively. The solid lines display fits using the swollen nanoparticle form factor.

To further investigate nanoparticles of PLGPβCD4 and D70HxAda, mixes where the βCD:Ada molar ratios were 2.3:1 and 1:2.3 (mix 2 and 3, respectively, prepared by mixing 2.3:1 and 1:2.3

(v/v) of the PLGPβCD4 and D70HxAda solutions used to prepare mix 1 as described above) were also analyzed using SAXS, cf. figure 4 for the scattering intensity of mix 1-3. As seen from the scattering curves, both mix 1 and 2 display a hint of a plateau in the scattered intensity (log-log representation) at low Q, indicating a Guinier regime and thus nanoparticles with finite sizes rather than random aggregation. Mix 3, on the other hand, show ill-defined aggregates with a typical Q^{-4} behavior indicative of macroscopic phase separation, which is most likely caused by association of the excess adamantyl groups. Prior to fitting of the SAXS data, the amount of free polymer in the nanoparticle solutions was estimated by centrifuging the samples and subsequent analyzing the supernatant. This analysis provided 3, 6 and 15 wt. % free polymer for mix 1, 2 and 3, respectively, confirming that the free polymer contributes negligible to the scattered intensity, which was consequently ignored in the analysis.

The data of mix 1 and 2 were analyzed using the indirect Fourier transform (IFT) routine(Glatter, 1977) implemented in the data program GNOM in the ATSAS package (Petoukhov et al., 2012). This model-independent approach provides an estimate of the overall symmetry and internal density distribution via the pair distribution function, p(r), describing the correlation between pairs of scattering points within the nanoparticle. As seen in figure 5, rather symmetric distributions are obtained thus indicating spherical structures for both nanoparticles. From this simple analysis we estimate max dimensions, i.e., maximum diameters, of about 90 and 80 nm for mix 1 and 2, respectively. The Gaussian distribution of assembly size, σ_D (equation 5 in section 2.3), was consequently found to be rather broad, with a standard deviation of about 18% for the stoichiometric 1:1 mixture (mix 1) while for mix 2 we find a broader distribution of about 22%.

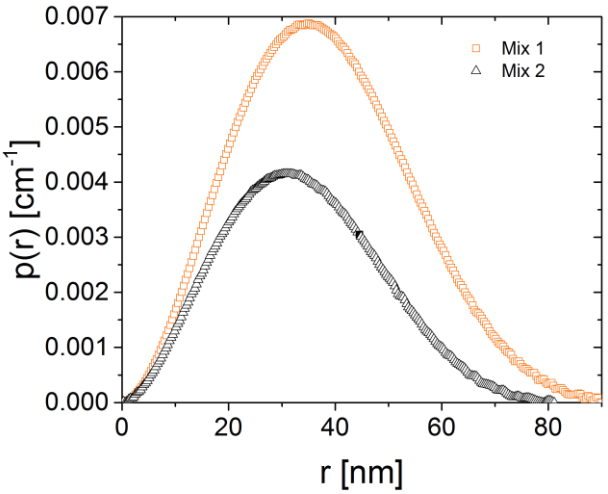

Fig. 5. The pair correlation function, p(r), obtained from the IFT analysis of the nanoparticles of mix 1 and 2.

In order to extract more detailed information, we proceeded to analyze the scattering data of mix 1 and 2 in figure 4 using a detailed scattering function for "fuzzy" spherical nanoparticles with a Gaussian polydispersity distribution (equation 9 in section 2.3). The results of this fit analysis are given in table 3 and displayed in figure 4 demonstrating an excellent description of the data. Performing the analysis on an absolute intensity scale, holding all molecular parameters such as concentration, density, electron density fixed to the predetermined values, we estimate the average M_{NA} of the assemblies to be $1.1 \cdot 10^8$ and $6.2 \cdot 10^7$ g mol^{-1} for mix 1 and mix 2, respectively. From the fits, we also find an overall radius, R_p, of 35 nm and 34 nm for mix 1 and 2, respectively. The latter values are slightly smaller than what was found from the model-independent IFT analysis ($D_{max}/2$ = 45 and 40 nm for mix 1 and 2, respectively), which can be attributed to the "rough" outer surface layer, σ_R, and size distribution, σ_D, indicating that an exact nanoparticle size is not easily defined.

Table 3. Fit parameters obtained from SAXS analysis and aggregation number (N_{agg}).

	M_{NA} [g mol^{-1}]	N_{agg}*	R_p [nm]	σ_R [nm]	I_0 [cm^{-1}]	ξ [nm]	σ_{PD} [%]
Mix 1	$1.1 \cdot 10^8$	174:709	35	1.2	0.05	5	18
Mix 2	$6.2 \cdot 10^7$	137:239	34	1.5	0.03	11	22

*The N_{agg} is given as PLGPβCD4:D70HxAda and calculated assuming that the host:guest molar ratios in the assemblies are 1:1 and 2.3:1 for mix 1 and 2, respectively.

In order to illustrate the nanoparticle structure and size distribution, we plotted the normalized internal density distribution, n(r) (equation 8 in section 2.3), together with the found overall size distribution, f(r) (equation 5 in section 2.3), in terms of the outer radius R_p, and the width, σ_{PD}, given in table 3. As directly seen from the plot in figure 6, the nanoparticles are not compact, but contains a significant amount of water, which can be attributed to the numerous hydrogen bond donors and acceptors in the glucose units. Not surprisingly, the stoichiometrically mixed sample (mix 1) is more compact and the nanoparticles contain approx. 75% polymer on average as compared to 45% for mix 2.

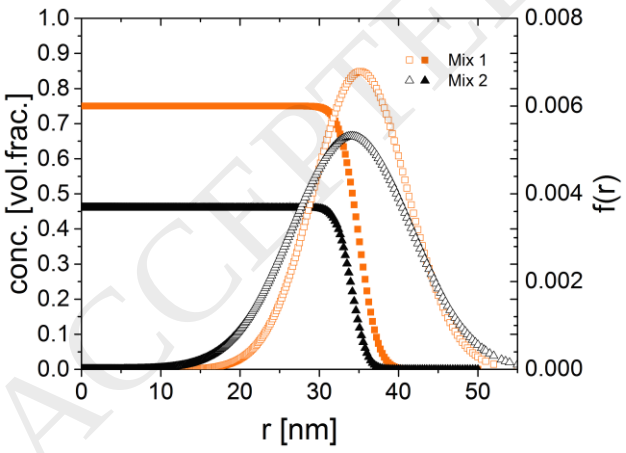

Fig. 6. The normalized internal density distribution given as concentration in volume fraction, n(r) (solid points), and overall size distribution, f(r) (open points), of the nanoparticles obtained using SAXS.

The internal structure, or "porosity", can also be determined from the scattering curves in figure 4 at high Q as excess scattering. From the SAXS fits, we extracted the correlation length, ξ, of the internal polymer network of the nanoparticle. Although the results are subjected to some uncertainty in background subtraction, the fit analyses indicate ξ-values of about 5 and 11 nm for mix 1 and mix 2, respectively. This finding is consistent with the larger amount of solvent in mix 2, and thus suggests a less rigid structure of the nanoparticles of mix 2, i.e. larger porosity. The results of mix 1 can be compared to those of a recent study where βCD-modified dextran (dextran backbone 70 kg mol^{-1} and 16 mole % modification of the glucose units of the backbone) was stoichiometrically mixed with an adamantane-modified dextran (dextran backbone 40 kg mol^{-1} and 9 mole % modification directly, i.e., no spacer, on the glucose units of the backbone) (Antoniuk et al., 2017). Similar features are observed for the nanoparticles in terms of R_g and size distribution, however the correlation lengths (ξ of 2.1 – 2.4 nm) are about 2 times lower than in the current study (5 nm), which is most likely explained by the higher intrinsic rigidity of pullulan and the lack of spacer between adamantyl and the 40 kg mol^{-1} dextran. Moreover, the larger degree of βCD modification of the pullulan, as compared to the βCD-modified dextran (25 and 16 mole % modification, respectively), may result in an additional effect of mobility decrease.

4. Conclusion

A series of βCD-pullulans (6.5 – 23.6 mole % βCD modification of the glucose units) and an adamantane-modified dextran (9.2 mole % adamantane modification of the glucose units) were prepared using "click" chemistry. Despite established synthesis protocols and attractive properties of pullulan, the βCD-pullulans are the first examples of well-defined linear polymers

obtained by grafting of cyclodextrins onto pullulan. The successful synthesis was verified using NMR and GFC. SAXS analysis of the polymers revealed clustering of the hydrophobically modified dextran. This is difficult to see from routine polymer characterization methods, thus emphasizing the strong potential of SAXS as a complementary polymer characterization method. ITC showed excellent binding properties of the cyclodextrin moieties with binding affinities close to that of native βCD.

Well-defined nanoparticles were created via host-guest interactions in aqueous solution. From DLS and detailed SAXS investigations, we showed how the molecular structure of the polymers and the βCD:adamantyl mixing ratios affect the structural properties of the nanoparticles. For example, that the nanoparticle size decrease with increasing degree of modification of the βCD-pullulans and that the βCD:adamantyl ratio is important in terms of stability towards aggregation, and strongly influence the inner porosity of the nanoparticles. An excess of adamantyl leads to aggregation, whereas equimolar ratio and an excess of βCD lead to well-defined particles.

The presented work contributes to unravel the connection between the molecular design of host:guest polysaccharides and the properties of the resulting nanoparticles. Such understanding is expected to significantly aid in the tailoring of host:guest nanoparticles, where e.g., size, dissociation, aggregation and release profile should be controlled. Moreover, the novel βCD-pullulan based nanoparticles (size of 70-100 nm) may be promising as targeted drug delivery vehicles, e.g., through the bloodstream towards the liver and possibly via the enhanced permeation and retention (EPR) effect, in cancer therapy.

Acknowledgements

The authors greatly appreciate the financial support of the Augustinus Foundation, and of the European Union through the NanoS3 project (GrantNo. 290251) of the FP7-PEOPLE-2011-ITN call.

Appendix A. Supplementary data

- Detailed synthesis conditions
- NMR data
- ITC enthalpograms
- SAXS scattering length densities

This material is available free of charge via the Internet at http://pubs.acs.org.

References

Alsbaiee, A., Smith, B. J., Xiao, L., Ling, Y., Helbling, D. E., & Dichtel, W. R. (2016). Rapid removal of organic micropollutants from water by a porous β-cyclodextrin polymer. *Nature,* 529(7585), 190.

Antoniuk, I., Plazzotta, B., Wintgens, V., Volet, G., Nielsen, T. T., Pedersen, J. S., & Amiel, C. (2017). host–guest interaction and structural ordering in polymeric nanoassemblies: Influence of molecular design. *International Journal of Pharmaceutics,* 531(2), 433-443.

Beaucage, G. (1996). Small-angle scattering from polymeric mass fractals of arbitrary mass-fractal dimension. *Journal of Applied Crystallography,* 29(2), 134-146.

Bender, H., Lehmann, J., & Wallenfels, K. (1959). Pullulan, ein extracelluläres Glucan von Pullularia pullulans. *Biochimica et Biophysica Acta,* 36(2), 309-316.

Brant, D. A., Liu, H.-S., & Zhu, Z. S. (1995). The dependence of glucan conformational dynamics on linkage position and stereochemistry. *Carbohydrate Research,* 278(1), 11-26.

Bruneel, D., & Schacht, E. (1995). Enzymatic degradation of pullulan and pullulan derivatives. *Journal of Bioactive and Compatible Polymers,* 10(4), 299-312.

Buliga, G. S., & Brant, D. A. (1987). Theoretical interpretation of the unperturbed aqueous solution configuration of pullulan. *International Journal of Biological Macromolecules,* 9(2), 77-86.

Burton, B. A., & Brant, D. A. (1983). Comparative flexibility, extension, and conformation of some simple polysaccharide chains. *Biopolymers,* 22(7), 1769-1792.

Chan, T. R., Hilgraf, R., Sharpless, K. B., & Fokin, V. V. (2004). Polytriazoles as copper(I)-stabilizing ligands in catalysis. *Organic Letters,* 6(17), 2853-2855.

Charlot, A., Heyraud, A., Guenot, P., Rinaudo, M., & Auzély-Velty, R. (2006). Controlled synthesis and inclusion ability of a hyaluronic acid derivative bearing β-cyclodextrin molecules. *Biomacromolecules,* 7(3), 907-913.

Dais, P., Vlachou, S., & Taravel, F. R. (2001). 13C nuclear magnetic relaxation study of segmental dynamics of the heteropolysaccharide pullulan in dilute solutions. *Biomacromolecules,* 2(4), 1137-1147.

Foot, J. S., Lui, F. E., & Kluger, R. (2009). Hemoglobin bis-tetramers via cooperative azide–alkyne coupling. *Chemical Communications*(47), 7315-7317.

Fundueanu, G., Constantin, M., Mihai, D., Bortolotti, F., Cortesi, R., Ascenzi, P., & Menegatti, E. (2003). Pullulan–cyclodextrin microspheres: a chromatographic approach for the evaluation of the drug–cyclodextrin interactions and the determination of the drug release profiles. *Journal of Chromatography B,* 791(1-2), 407-419.

Glatter, O. (1977). A new method for the evaluation of small-angle scattering data. *Journal of Applied Crystallography,* 10(5), 415-421.

Gomez, C. G., Chambat, G., Heyraud, A., Villar, M., & Auzély-Velty, R. (2006). Synthesis and characterization of a β-CD-alginate conjugate. *Polymer,* 47(26), 8509-8516.

Gottlieb, H. E., Kotlyar, V., & Nudelman, A. (1997). NMR chemical shifts of common laboratory solvents as trace impurities. *The Journal of Organic Chemistry,* 62(21), 7512-7515.

Jia, Y.-G., & Zhu, X. (2014). Self-healing supramolecular hydrogel made of polymers bearing cholic acid and β-cyclodextrin pendants. *Chemistry of Materials,* 27(1), 387-393.

K Osman, S., M Soliman, G., & Abd El Rasoul, S. (2015). Physically Cross-linked Hydrogels of β-cyclodextrin Polymer and Poly (ethylene glycol)-cholesterol as Delivery Systems for Macromolecules and Small Drug Molecules. *Current Drug Delivery,* 12(4), 415-424.

Kadkhodaei, M., Wu, H., & Brant, D. A. (1991). Comparison of the conformational dynamics of the (1→ 4)-and (1→ 6)-linked αD-glucans using 13C-NMR relaxation. *Biopolymers,* 31(13), 1581-1592.

Kakuta, T., Takashima, Y., & Harada, A. (2013). Highly elastic supramolecular hydrogels using host–guest Inclusion complexes with cyclodextrins. *Macromolecules,* 46(11), 4575-4579.

Kaneo, Y., Tanaka, T., Nakano, T., & Yamaguchi, Y. (2001). Evidence for receptor-mediated hepatic uptake of pullulan in rats. *Journal of Controlled Release,* 70(3), 365-373.

Layre, A.-M., Volet, G., Wintgens, V., & Amiel, C. (2009). Associative network based on cyclodextrin polymer: a model system for drug delivery. *Biomacromolecules,* 10(12), 3283-3289.

Lu, L., Shao, X., Jiao, Y., & Zhou, C. (2014). Synthesis of chitosan-graft-β-cyclodextrin for improving the loading and release of doxorubicin in the nanopaticles. *Journal of Applied Polymer Science,* 131(21).

Machín, R., Isasi, J. R., & Vélaz, I. (2012). β-Cyclodextrin hydrogels as potential drug delivery systems. *Carbohydrate Polymers,* 87(3), 2024-2030.

Malik, N. S., Ahmad, M., & Minhas, M. U. (2017). Cross-linked β-cyclodextrin and carboxymethyl cellulose hydrogels for controlled drug delivery of acyclovir. *PLOS one,* 12(2), e0172727.

Mitha, A., & Rekha, M. (2014). Multifunctional polymeric nanoplexes for anticancer co-delivery of p53 and Mitoxantrone. *Journal of Materials Chemistry B,* 2(45), 8005-8016.

Morin-Crini, N., Winterton, P., Fourmentin, S., Wilson, L. D., Fenyvesi, É., & Crini, G. (2018). Water-insoluble β-cyclodextrin–epichlorohydrin polymers for removal of pollutants from aqueous solutions by sorption processes using batch studies: A review of inclusion mechanisms. *Progress in Polymer Science,* 78, 1-23.

Nielsen, T. T., Wintgens, V., Amiel, C., Wimmer, R., & Larsen, K. L. (2010). Facile synthesis of β-cyclodextrin-dextran polymers by "click" chemistry. *Biomacromolecules,* 11(7), 1710-1715.

Pernot, P., Round, A., Barrett, R., De Maria Antolinos, A., Gobbo, A., Gordon, E., . . . Mattenet, M. (2013). Upgraded ESRF BM29 beamline for SAXS on macromolecules in solution. *Journal of Synchrotron Radiation,* 20(4), 660-664.

Petoukhov, M. V., Franke, D., Shkumatov, A. V., Tria, G., Kikhney, A. G., Gajda, M., . . . Svergun, D. I. (2012). New developments in the ATSAS program package for small-angle scattering data analysis. *Journal of Applied Crystallography,* 45(2), 342-350.

Rekha, M. R., & Sharma, C. P. (2011). Hemocompatible pullulan-polyethyleneimine conjugates for liver cell gene delivery: In vitro evaluation of cellular uptake, intracellular trafficking and transfection efficiency. *Acta Biomater,* 7(1), 370-379.

Rekharsky, M. V., & Inoue, Y. (1998). Complexation thermodynamics of cyclodextrins. *Chemical Reviews,* 98(5), 1875-1918.

Rostovtsev, V. V., Green, L. G., Fokin, V. V., & Sharpless, K. B. (2002). A stepwise huisgen cycloaddition process: copper (I)-catalyzed regioselective "ligation" of azides and terminal alkynes. *Angewandte Chemie,* 114(14), 2708-2711.

Shingel, K. I. (2004). Current knowledge on biosynthesis, biological activity, and chemical modification of the exopolysaccharide, pullulan. *Carbohydrate Research,* 339(3), 447-460.

Singh, R. S., Kaur, N., Rana, V., & Kennedy, J. F. (2017). Pullulan: a novel molecule for biomedical applications. *Carbohydrate Polymers,* 171, 102-121.

Takashima, Y., Hatanaka, S., Otsubo, M., Nakahata, M., Kakuta, T., Hashidzume, A., . . . Harada, A. (2012). Expansion–contraction of photoresponsive artificial muscle regulated by host–guest interactions. *Nature Communications,* 3, 1270.

Tanaka, T., Fujishima, Y., Hanano, S., & Kaneo, Y. (2004). Intracellular disposition of polysaccharides in rat liver parenchymal and nonparenchymal cells. *International Journal of Pharmaceutics,* 286(1-2), 9-17.

Tornøe, C. W., Christensen, C., & Meldal, M. (2002). Peptidotriazoles on solid phase:[1, 2, 3]-triazoles by regiospecific copper (I)-catalyzed 1, 3-dipolar cycloadditions of terminal alkynes to azides. *The Journal of Organic Chemistry,* 67(9), 3057-3064.

Trotta, F., Zanetti, M., & Cavalli, R. (2012). Cyclodextrin-based nanosponges as drug carriers. *Beilstein Journal of Organic Chemistry,* 8(1), 2091-2099.

Wang, Z., Zhang, P., Hu, F., Zhao, Y., & Zhu, L. (2017). A crosslinked β-cyclodextrin polymer used for rapid removal of a broad-spectrum of organic micropollutants from water. *Carbohydrate Polymers,* 177, 224-231.

Whistler, R. (2012). *Industrial gums: polysaccharides and their derivatives*: Elsevier.

Wintgens, V., Nielsen, T. T., Larsen, K. L., & Amiel, C. (2011). Size-controlled nanoassemblies based on cyclodextrin-modified dextrans. *Macromolecular Bioscience,* 11(9), 1254-1263.

Xiao, L., Ling, Y., Alsbaiee, A., Li, C., Helbling, D. E., & Dichtel, W. R. (2017). β-Cyclodextrin polymer network sequesters perfluorooctanoic acid at environmentally relevant concentrations. *Journal of the American Chemical Society,* 139(23), 7689-7692.